International Journal of Engineering, Science and Environment
Peer-Reviewed Open Access • CC BY 4.0 • Quarterly
ijese.in

e-ISSN: 2839-5360
Vol. 1 | Issue 2 | Jul–Sep 2026

RESEARCH ARTICLE
Received: 02 July 2026 | Accepted: 27 September 2026 | Published: 30 September 2026

A Fluid-Dynamic Framework for Carbon Dioxide Removal: Nonlinear Dynamics, Stability, and Optimal Operation

Lakshmi N. Sridhar*

Chemical Engineering Department, University of Puerto Rico, Mayaguez, PR 00681

***Corresponding Author:** lakshmin.sridhar@upr.edu

ABSTRACT

Carbon dioxide removal (CDR) technologies are increasingly recognized as essential components of global climate mitigation strategies to reduce atmospheric greenhouse gas concentrations. The performance of many carbon dioxide removal systems is strongly influenced by fluid transport, mixing, and nonlinear flow interactions, making fluid mechanics a critical aspect of their design and operation. In this study, a reduced-order fluid-dynamic model for carbon dioxide removal is developed and analyzed using nonlinear dynamical systems techniques. The model consists of three coupled nonlinear ordinary differential equations representing dominant transport modes and an external forcing parameter associated with system operation. Numerical continuation is performed to investigate the equilibrium structure and identify critical operating conditions. The analysis reveals a supercritical Hopf bifurcation and a limit point, indicating oscillatory dynamics and multiple operating regimes. A limit cycle emerging from the Hopf bifurcation is also computed and characterized. To improve system performance, an optimal control problem is formulated in which the forcing parameter is treated as a time-dependent control variable. A stability-aware penalty based on a learned stability indicator is incorporated into the objective function to discourage operation near unstable regions. Numerical results demonstrate that the bifurcation-aware control strategy substantially changes the optimal solution and produces smoother control trajectories. The proposed framework provides new insights into the interactions among fluid dynamics, stability, and operational efficiency in carbon dioxide removal systems.

Keywords: Carbon dioxide removal, Environmental fluid mechanics, Reduced-order modeling, Hopf bifurcation, Optimal control

1. INTRODUCTION

The increasing concentration of atmospheric carbon dioxide (CO_2) has emerged as one of the most significant environmental challenges of the twenty-first century. Anthropogenic emissions from fossil fuel combustion, industrial activities, transportation, and land-use changes have substantially contributed to global climate change, leading to rising temperatures, extreme weather events, sea-level rise, and ecosystem degradation. As nations strive to achieve net-zero emission targets and meet international climate commitments, carbon dioxide removal technologies have become an essential component of long-term climate mitigation strategies. While renewable energy deployment and energy-efficiency improvements can reduce future emissions, large-scale carbon dioxide removal is increasingly recognized as necessary to address residual emissions and reduce existing atmospheric CO_2 concentrations.

Carbon dioxide removal encompasses a broad range of technologies and processes designed to capture CO_2 either directly from emission sources or from the atmosphere itself. These technologies include post-combustion capture, direct air capture, geological sequestration, mineral carbonation, bioenergy with carbon capture and storage, and ocean-based carbon removal approaches. Regardless of the specific technology employed, fluid mechanics plays a central role in determining system performance. The transport of carbon dioxide through gases, liquids, porous media, and reactive environments is fundamentally governed by fluid flow, mixing, convection, diffusion, and mass transfer processes. Consequently, understanding the fluid-dynamic mechanisms that influence carbon dioxide transport is critical for the design and optimization of efficient carbon removal systems.

Environmental engineering applications involving carbon dioxide removal frequently involve highly coupled transport phenomena. In direct air capture systems, atmospheric air must be transported through sorbent contactors where fluid flow characteristics determine residence times and capture efficiency. In absorption-based systems, gas-liquid interactions control mass transfer rates and ultimately influence the amount of carbon dioxide removed from flue gases. Geological carbon sequestration involves the injection of supercritical carbon dioxide into deep saline aquifers or depleted hydrocarbon reservoirs, where buoyancy-driven flow, density gradients, and porous-media transport govern plume migration and long-term storage security. Similarly, mineral carbonation and reactive transport processes depend strongly on the interaction between fluid flow and chemical reactions. These examples illustrate the fundamental importance of fluid mechanics across a wide spectrum of carbon dioxide removal technologies.

The complexity of fluid-dynamic phenomena in carbon dioxide removal systems often necessitates the use of advanced computational models. High-fidelity computational fluid dynamics (CFD) simulations have become valuable tools for investigating transport processes, mixing behavior, and flow structures in carbon capture systems. However, such models are frequently computationally expensive and may be impractical for tasks requiring repeated simulations, optimization studies, control design, or stability analysis. As a result, there is growing interest in the development of reduced-order models that retain the dominant physical mechanisms while significantly reducing computational complexity.

How to cite: L. N. Sridhar, "A Fluid-Dynamic Framework for Carbon Dioxide Removal: Nonlinear Dynamics, Stability, and Optimal Operation," Int. J. Eng. Sci. Environ., vol. 1, no. 2, pp. 11–25, 2026.
Copyright © 2026 The Author(s). Open access article under the CC BY 4.0 licence (https://creativecommons.org/licenses/by/4.0/), permitting unrestricted use with proper citation.

Reduced-order modeling provides an attractive framework for capturing the essential dynamics of complex fluid systems using a limited number of governing variables, thereby enabling efficient analysis of system behavior over a wide range of operating conditions.

Reduced-order models have been successfully applied in numerous fluid mechanics applications, including turbulent flows, environmental transport systems, atmospheric dynamics, and flow control problems. These models provide valuable insight into the dominant mechanisms governing system behavior while facilitating mathematical analysis and optimization. In the context of carbon dioxide removal, reduced-order models can serve as efficient surrogates for large-scale simulations, allowing researchers to investigate the interaction between fluid transport, capture efficiency, and operational parameters. Furthermore, such models enable the application of nonlinear dynamical systems theory to study the stability and evolution of carbon removal processes.

An important characteristic of many environmental and fluid-dynamic systems is the presence of nonlinear feedback mechanisms. Interactions among transport processes, concentration fields, reaction rates, and external forcing can generate complex dynamic behavior that cannot be adequately described using purely steady-state approaches. Nonlinear systems may exhibit multiple equilibrium states, oscillatory behavior, threshold phenomena, and abrupt transitions between operating regimes. These features can significantly influence the effectiveness and reliability of carbon dioxide removal technologies. Consequently, understanding the dynamic behavior of carbon capture systems is essential for achieving stable and efficient operation.

Optimizing carbon dioxide removal systems is another major challenge in environmental engineering. Carbon capture technologies often require substantial energy for pumping, compression, regeneration, and circulation. Minimizing energy use while maintaining effective carbon removal is therefore a critical objective. Advanced optimization and control strategies offer promising approaches to improving system performance by determining operating policies that balance capture efficiency, energy requirements, and system stability. Developing reduced-order dynamic models provides a practical foundation for formulating these optimization problems and for exploring how operating conditions influence overall system behavior.

Motivated by these considerations, the present study develops a reduced-order fluid-dynamic model for carbon dioxide removal and investigates its dynamic characteristics. The model incorporates nonlinear interactions among dominant transport modes and an externally controlled forcing parameter representing operational intervention. The resulting dynamical system is capable of capturing important features associated with coupled transport processes while remaining computationally tractable. Numerical continuation techniques are employed to investigate the equilibrium structure and identify critical operating conditions associated with dynamic transitions. In addition, an optimal control framework is developed to determine operating strategies that minimize a performance objective while promoting efficient system operation.

The integration of reduced-order fluid-dynamic modeling, nonlinear dynamics, and optimal control provides a framework for investigating the stability and operational behavior of carbon dioxide removal systems. The present study focuses specifically on identifying critical dynamical transitions and developing control strategies that avoid unstable operating regimes.

2. LITERATURE REVIEW

2.1. Carbon Dioxide Removal and Capture

Carbon dioxide capture and removal technologies have become increasingly important due to growing concerns regarding atmospheric greenhouse gas concentrations and climate change mitigation. Early investigations emphasized the fundamental principles and economic aspects of carbon dioxide capture processes, highlighting the importance of efficient transport and separation mechanisms in large-scale deployment of carbon capture technologies [1].

Amine scrubbing, the most established of these CO_2 separation technologies, was later reviewed in detail [2].

2.2. Fluid Mechanics in Carbon Dioxide Capture

Research subsequently focused on the role of fluid mechanics in gas–liquid systems, where bubble breakup, coalescence, and interfacial transport were identified as key factors governing mass transfer rates in carbon dioxide absorption processes [3]. Studies of post-combustion carbon capture further demonstrated that fluid flow and mixing significantly influence absorption efficiency and overall process performance [4]. Fundamental investigations of gas solubility and diffusivity provided important information regarding the transport properties of carbon dioxide in aqueous solutions, which are critical for predicting capture rates and reactor behavior [5]. At the same time, attention was directed toward underground carbon storage, where fluid migration mechanisms within geological formations were recognized as important factors affecting long-term sequestration performance [6].

Subsequent reviews examined carbon capture and storage technologies more broadly, including the transport phenomena that influence carbon dioxide removal efficiency [7]. The fluid mechanics of carbon dioxide sequestration was later analyzed in detail, establishing the importance of buoyancy-driven flow, density variations, and convective transport in subsurface storage systems [8]. The coupling between geochemical reactions and convective mixing in geological storage formations was investigated to understand how fluid flow influences the long-term stability of stored carbon dioxide [9].

Research on sequestration in deep sedimentary formations further highlighted the importance of multiphase flow processes, permeability distributions, and fluid transport pathways in determining storage effectiveness [10]. Comprehensive assessments of carbon dioxide capture and storage technologies provided a broad overview of capture methods, transport systems, geological storage mechanisms, and associated engineering challenges [11]. Fluid mechanical

© 2026 The Author(s) Licensed under CC BY 4.0 | Published by Engineering, Science and Environmental Research Publications | e-ISSN 2839-5360 | ijese.in

studies of carbon dioxide storage in saline aquifers demonstrated that convection-driven mixing can significantly enhance dissolution and improve storage security [12].

2.3. Computational Research in Carbon Dioxide Capture

The migration of carbon dioxide plumes within porous geological formations was investigated through mathematical and computational models, revealing the importance of buoyancy, permeability, and density contrasts in controlling plume evolution [13]. Additional studies examined the impact of relative permeability hysteresis on storage performance and showed that multiphase flow effects strongly influence carbon dioxide trapping efficiency [14].

2.4. Technology in Carbon Dioxide Capture

Long-term assessments of carbon capture and storage technologies indicated that storage capacity and transport mechanisms play a central role in determining the viability of carbon sequestration as a climate mitigation strategy [15]. Interest subsequently expanded beyond storage toward direct carbon dioxide removal from the atmosphere, with thermodynamic analyses providing insight into the energy requirements of direct air capture processes [16]. Further developments in direct air capture technology demonstrated the feasibility of extracting carbon dioxide directly from ambient air through engineered contactor systems designed to maximize mass transfer and fluid–surface interactions [17]. Geological storage studies continued to emphasize the importance of subsurface fluid mechanics and transport processes in maintaining long-term storage security [18]. Research addressing the large-scale deployment of carbon capture technologies highlighted challenges associated with process intensification, fluid handling, and transport efficiency [19]. Numerical simulations of carbon dioxide plume migration in geological formations provided additional understanding of the influence of fluid flow and reservoir heterogeneity on storage behavior [20]. Direct air capture technologies attracted considerable attention due to their potential role in negative emissions strategies. Comprehensive reviews examined sorbent materials, contactor configurations, and fluid dynamic considerations governing carbon dioxide transport from the atmosphere to capture surfaces [21]. Experimental investigations also demonstrated the rapid mineralization of carbon dioxide in basaltic formations, providing an alternative pathway for permanent carbon storage through reactive transport processes [22].

2.5. Theoretical Transport Phenomena in Carbon Dioxide Capture

Theoretical developments in porous-media convection contributed significantly to the understanding of fluid transport within geological storage systems, providing analytical and numerical tools for describing buoyancy-driven flow and mass transfer phenomena [23]. Studies of turbulent atmospheric mixing further emphasized the role of fluid motion in governing the transport and distribution of carbon dioxide across environmental systems [24]. Comprehensive analyses of carbon capture technologies examined fluid transport, absorption processes, membrane systems, adsorption mechanisms, and storage strategies, highlighting the central role of fluid mechanics across the entire carbon capture chain [25]. Evaluations of negative-emission technologies subsequently investigated the energy and transport requirements associated with large-scale carbon dioxide removal, identifying fluid transport processes as critical determinants of system efficiency [26].

2.6. Recent Studies

Recent studies have explored the integration of carbon capture and removal technologies into future net-zero energy systems [27]. Fluidized-bed carbon capture technologies have emerged as promising alternatives due to their superior gas–solid contact characteristics and enhanced mass transfer performance [28]. The most recent assessments of carbon dioxide removal have highlighted the growing importance of engineered carbon removal systems [29]. These studies collectively indicate that fluid mechanics remains one of the fundamental scientific disciplines underlying the design, operation, and optimization of carbon dioxide removal technologies. Beyond CO_2 capture and permanent storage, downstream carbon utilization provides a complementary pathway in which captured CO_2 can be converted into value-added products. For example, Parkash et al. [30] demonstrated electrochemical CO_2 reduction to ethanol using copper-deposited basalt fiber fabric. Although such electrochemical conversion is outside the scope of the reduced-order fluid-dynamic model developed in the present study, it illustrates the broader process context in which efficient and stable CO_2 capture can be coupled with subsequent utilization. The present work therefore focuses on the upstream fluid-transport, stability, and control aspects of CO_2 removal, which may ultimately support integration with either storage or utilization pathways.

Overall, the existing literature demonstrates that carbon dioxide removal systems are governed by a complex interplay of fluid flow, transport phenomena, mixing processes, convection, and mass transfer. While substantial progress has been achieved in understanding these mechanisms, there remains a need for computationally efficient dynamical models capable of linking fluid-mechanical behavior with system-level performance. The present work addresses this need through the development of a reduced-order fluid-dynamic framework that captures the essential transport interactions governing carbon dioxide removal while providing a foundation for stability analysis and control-oriented investigations.

3. MAIN OBJECTIVES OF THIS WORK

The primary objective of this work is to develop and analyze a reduced-order nonlinear dynamical model that captures the essential flow–transport interactions governing carbon dioxide removal processes. By representing the dominant dynamics through a low-dimensional system of ordinary differential equations, the study seeks to provide a computationally efficient framework for investigating the stability, bifurcation behavior, and control characteristics of CO_2 removal systems.

A second objective is to identify and characterize the nonlinear dynamical features of the system through bifurcation analysis.

© 2026 The Author(s) Licensed under CC BY 4.0 | Published by Engineering, Science and Environmental Research Publications | e-ISSN 2839-5360 | ijese.in

Particular emphasis is placed on determining the existence and location of Hopf and limit point bifurcations, understanding the transition from steady-state operation to oscillatory behavior, and analyzing the stability of equilibrium solutions. This objective aims to reveal the critical operating conditions that influence the efficiency and robustness of carbon dioxide removal processes.

The third objective is to investigate the oscillatory dynamics that emerge near the Hopf bifurcation point and to examine the associated limit cycle behavior. Understanding these oscillations is important because periodic fluctuations in flow and concentration fields can adversely affect carbon capture performance and increase operational complexity.

A fourth objective is to formulate and solve an optimal control problem in which the external forcing parameter is treated as a time-dependent control variable. The goal is to determine control policies that minimize a performance index based on state magnitudes and control effort while maintaining favorable operating conditions.

The fifth objective is to incorporate bifurcation-awareness into the optimal control framework through a stability-based penalty mechanism. This enables the optimization procedure to avoid regions of the state space associated with Hopf instability, thereby promoting dynamically stable operation.

Finally, the study aims to evaluate the effectiveness of stability-aware optimal control by comparing system performance with and without the stability penalty.

Through this comparison, the work seeks to demonstrate how stability-informed control can improve efficiency, reduce oscillatory behavior, lower control effort, and enhance the overall performance of carbon dioxide removal systems.

The novelty of this work lies in the integration of nonlinear dynamical systems theory, bifurcation analysis, machine-learning-assisted stability prediction, and optimal control within a unified framework for carbon dioxide removal.

Previous studies on carbon dioxide capture and removal have extensively investigated transport and mass-transfer phenomena, absorption and adsorption processes, reactor and process design, and process optimization. In contrast, the present work focuses specifically on nonlinear dynamical instabilities, bifurcation behavior, and their incorporation into stability-aware optimal control.

A key novel aspect of this study is the development of a reduced-order nonlinear model that captures the essential interactions between flow dynamics, carbon dioxide transport, and auxiliary stabilization mechanisms. The model is sufficiently simple to permit detailed dynamical analysis while retaining the nonlinear coupling required to generate complex behaviors such as Hopf bifurcations, limit cycles, and multiple equilibrium states. This enables the direct investigation of stability transitions that are often difficult to study using large-scale computational fluid dynamics models.

A second major contribution is the identification and characterization of a supercritical Hopf bifurcation within the carbon dioxide removal framework. The study demonstrates how oscillatory behavior can emerge through nonlinear flow–transport interactions and establishes the associated limit cycle dynamics. This provides new insight into the mechanisms that can lead to periodic fluctuations in carbon capture performance and highlights the importance of considering dynamic stability during system operation.

Another novel feature is the incorporation of bifurcation information directly into the optimal control problem. Rather than optimizing system performance solely on the basis of state variables and control effort, the proposed framework introduces a stability-aware penalty that discourages trajectories approaching regions of Hopf instability. This transforms the optimization problem from a conventional control formulation into a bifurcation-aware optimal control strategy capable of simultaneously improving performance and maintaining dynamic stability.

The work is further distinguished by the use of a neural-network-based stability surrogate trained from continuation data generated using MATCONT. This approach eliminates the need for repeated eigenvalue calculations during optimization while preserving information regarding stability boundaries. The resulting hybrid framework combines continuation methods, machine learning, and nonlinear optimal control within a computationally efficient methodology.

Finally, the study demonstrates that incorporating bifurcation-awareness into the optimization process produces a substantially different optimal solution and significantly smoother control trajectories. This establishes a direct quantitative link between dynamical stability and operational efficiency in carbon dioxide removal systems. To the best of the author's knowledge, the combined use of reduced-order fluid-dynamic modeling, Hopf bifurcation analysis, machine-learning-based stability prediction, and bifurcation-constrained optimal control for carbon dioxide removal has not been reported previously. The proposed framework therefore provides a new approach for the design, analysis, and operation of dynamically stable and energy-efficient carbon capture systems.

The rest of this paper is organized as follows. First, the model equations are presented, followed by a description of the numerical procedures used. The results, discussion and conclusions are then presented in Sections 6–8.

4. MODEL EQUATIONS

The model represents a reduced-order description of carbon dioxide removal dynamics driven by coupled fluid transport and scalar concentration interactions. It captures the essential interplay between flow-induced mixing, CO_2 accumulation, and nonlinear saturation effects using a low-dimensional dynamical system. The first equation describes the evolution of the dominant transport mode, incorporating linear growth, nonlinear self-limiting behavior, coupling with CO_2 concentration, and external operational forcing. The second equation governs the CO_2 concentration mode, reflecting advective enhancement by fluid motion, nonlinear saturation due to finite absorption capacity, and feedback from auxiliary transport mechanisms. The third equation represents a stabilizing or delayed response mode that accounts for

© 2026 The Author(s) Licensed under CC BY 4.0 |

dissipation, regeneration effects, and nonlinear damping induced by strong flow activity. Together, these equations model the feedback structure between transport intensity and removal efficiency in environmental fluid systems. The nonlinear coupling terms enable complex dynamic behavior including multistability and oscillatory states. The external forcing parameter provides a means of controlling system behavior and represents practical operational interventions. Overall, the model provides a compact representation of key physical processes governing carbon dioxide removal. It serves as a foundation for bifurcation analysis and optimal control design in environmentally relevant fluid dynamic systems.

At the continuum level, the fluid motion and CO_2 transport are represented by the incompressible Navier--Stokes equations coupled with an advection--diffusion--reaction equation. The governing equations are

$$\begin{aligned}&\frac{\partial \mathbf{u}}{\partial t}+(\mathbf{u}\cdot\nabla)\mathbf{u}=-\nabla p+\nu\nabla^2\mathbf{u}+\mathbf{F}(c)+Q\mathbf{f},\nabla\cdot\mathbf{u}=0,\\&\frac{\partial c}{\partial t}+\mathbf{u}\cdot\nabla c=D\nabla^2 c+R(c,\mathbf{u})\end{aligned} \tag{1}$$

Here, $\mathbf{u}(\mathbf{x},t)$ is the velocity field, p is the pressure, $c(\mathbf{x},t)$ is the CO_2 concentration field, ν is the kinematic viscosity, D is the CO_2 diffusivity, $\mathbf{F}(c)$ represents the coupling between the concentration field and fluid motion, $R(c,\mathbf{u})$ represents reaction or absorption effects, and $Q\mathbf{f}$ represents the external operational forcing, such as pumping, injection, or suction.

To obtain a computationally tractable reduced-order representation, the velocity and CO_2 concentration fields are expanded in a finite set of spatial basis functions. The modal expansions are written as

$$\mathbf{u}(\mathbf{x},t)=\mathbf{u}_0(\mathbf{x})+\sum_{i=1}^{N_u}a_i(t)\phi_i(\mathbf{x}), \tag{2}$$

and

$$c(\mathbf{x},t)=c_0(\mathbf{x})+\sum_{j=1}^{N_c}b_j(t)\psi_j(\mathbf{x}), \tag{3}$$

where $\mathbf{u}_0$ and c_0 denote reference fields, ϕ_i and ψ_j are the selected spatial basis functions, and $a_i(t)$ and $b_j(t)$ are the corresponding time-dependent modal coefficients. The Galerkin projection is carried out by substituting the modal expansions into the governing continuum equations and requiring the residual to be orthogonal to the retained basis functions. The spatial inner product is defined as

$$\langle f,g\rangle=\int_\Omega f(\mathbf{x})g(\mathbf{x})d\Omega \tag{4}$$

For the dominant fluid-transport mode, we retain the approximation

$$\mathbf{u}(\mathbf{x},t)=\mathbf{u}_0(\mathbf{x})+a_1(t)\phi_1(\mathbf{x}), \tag{5}$$

while the dominant carbon dioxide concentration mode is represented by

$$c(\mathbf{x},t)=c_0(\mathbf{x})+a_2(t)\psi_1(\mathbf{x}) \tag{6}$$

An additional modal amplitude $a_3(t)$ is introduced to represent the delayed dissipative or absorber-regeneration response. Substitution of these expansions into the momentum equation and projection onto ϕ_1 gives

$$\left\langle \phi_1,\frac{\partial \mathbf{u}}{\partial t}+(\mathbf{u}\cdot\nabla)\mathbf{u}+\nabla p-\nu\nabla^2\mathbf{u}-\mathbf{F}(c)-Q\mathbf{f}\right\rangle=0 \tag{7}$$

Assuming that the basis functions are normalized such that

$$\langle\phi_1,\phi_1\rangle=1 \tag{8}$$

the time-dependent contribution becomes

$$\left\langle \phi_1,\frac{\partial \mathbf{u}}{\partial t}\right\rangle=\frac{da_1}{dt} \tag{9}$$

The projected linear, nonlinear, flow--concentration coupling, and forcing contributions are collected into reduced coefficients. These coefficients can be written generally as spatial projection integrals. For example,

$$\sigma=\langle\phi_1,\mathrm{L}_u(\phi_1)\rangle,\alpha_1=-\langle\phi_1,\mathrm{N}_u(\phi_1)\rangle,\alpha_2=-\langle\phi_1,\mathrm{C}_{uc}(\phi_1,\psi_1)\rangle,q_1=\langle\phi_1,\mathbf{f}\rangle \tag{10}$$

where L_u, N_u, and C_{uc} denote the projected linear, nonlinear, and flow--concentration coupling operators, respectively. Absorbing the forcing projection coefficient q_1 into the definition of the control variable Q gives the reduced dominant-mode equation

$$\frac{da_1}{dt}=\sigma a_1-\alpha_1 a_1^3-\alpha_2 a_1 a_2+Q \tag{11}$$

Similarly, projection of the carbon dioxide transport equation onto ψ_1 gives

$$\left\langle \psi_1,\frac{\partial c}{\partial t}+\mathbf{u}\cdot\nabla c-D\nabla^2 c-R(c,\mathbf{u})\right\rangle=0 \tag{12}$$

After collecting the projected linear, nonlinear, flow--concentration, and auxiliary-mode contributions, the concentration-mode equation becomes

$$\frac{da_2}{dt}=ra_2-\beta_1 a_2^3+\beta_2 a_1-\beta_3 a_3 \tag{13}$$

The coefficients r, β_1, β_2, and β_3 therefore represent the corresponding Galerkin projections of the linear concentration dynamics, nonlinear saturation, flow-induced transport, and coupling with the auxiliary mode. The auxiliary mode is represented by the modal amplitude $a_3(t)$ and is used to account for delayed transport, dissipation, or absorber-regeneration effects that are not explicitly resolved by the first two retained modes. Its reduced evolution equation is written as

$$\frac{da_3}{dt}=-qa_3+\gamma_1 a_2-\gamma_2 a_1^2 \tag{14}$$

Here, q represents the relaxation rate of the auxiliary mode, γ_1 represents coupling from the carbon dioxide concentration mode, and γ_2 represents nonlinear flow-induced damping. Collecting the three projected modal equations therefore yields the reduced-order system

International Journal of Engineering, Science and Environment
Peer-Reviewed Open Access • CC BY 4.0 • Quarterly
ijese.in
Vol. 1 | Issue 2 | Jul–Sep 2026

$$\frac{da_1}{dt} = \sigma a_1 - \alpha_1 a_1^3 - \alpha_2 a_1 a_2 + Q$$
$$\frac{da_2}{dt} = r a_2 - \beta_1 a_2^3 + \beta_2 a_1 - \beta_3 a_3 \quad (15)$$
$$\frac{da_3}{dt} = -q a_3 + \gamma_1 a_2 - \gamma_2 a_1^2$$

The reduced coefficients collect the spatially projected effects of transport, diffusion, nonlinear interactions, and intermodal coupling.

The state variables $a_1(t)$, $a_2(t)$, and $a_3(t)$ are signed, nondimensional reduced-order modal amplitudes rather than absolute values of fluid velocity, CO_2 concentration, or auxiliary transport quantities. Specifically, $a_1(t)$ represents the amplitude of the dominant fluid-transport mode, $a_2(t)$ represents the amplitude of the dominant CO_2 concentration/mixing mode, and $a_3(t)$ represents the amplitude of the auxiliary dissipative or regeneration mode. Because these variables describe modal contributions relative to their corresponding reference fields, their values may be either positive or negative. A negative modal amplitude indicates that the contribution of a particular mode is in the direction opposite to the corresponding basis function, or equivalently represents a negative deviation from the reference state. Therefore, a negative value of $a_1(t)$ does not imply a physically negative velocity magnitude, and a negative value of $a_2(t)$ does not imply a physically negative CO_2 concentration. The dimensional physical fields are reconstructed by combining the corresponding reference fields with the weighted modal contributions. Thus, negative values of $a_1(t)$, $a_2(t)$, or $a_3(t)$ appearing in the bifurcation diagrams and state trajectories are physically admissible within the reduced-order representation and should be interpreted as the direction and magnitude of the modal deviations from the reference state.

The velocity and concentration fields are approximated using modal expansions of the form

$$\mathbf{u}(x,t) \approx a_1(t)\phi_1(x), c(x,t) \approx a_2(t)\psi_1(x) \quad (16)$$

with an additional auxiliary mode introduced to capture delayed transport and stabilizing feedback mechanisms,

$$z(x,t) \approx a_3(t)\chi_1(x). \quad (17)$$

Here, $a_1(t)$ represents the dominant fluid transport or shear intensity mode, $a_2(t)$ represents the dominant CO_2 concentration or mixing mode, and $a_3(t)$ represents a secondary dissipative or absorber-regeneration mode that captures lagged system response effects commonly observed in environmental flow-reactive systems. Substituting these expansions into the governing equations and applying a Galerkin projection onto each basis function yields a set of coupled ordinary differential equations governing the temporal evolution of the modal amplitudes. The nonlinear terms arising from convective transport and reaction kinetics manifest as polynomial interactions between the modal amplitudes. In particular, self-interaction of the dominant flow mode generates cubic saturation effects due to energy redistribution and nonlinear dissipation, leading to a term proportional to $-a_1^3$. Similarly, coupling between flow and concentration modes produces bilinear interaction terms of the form a_1, a_2, representing the enhancement or suppression of CO_2 transport by fluid motion. External operational intervention, such as pumping, suction, or controlled injection in a carbon removal device, is represented through a forcing parameter Q, which enters additively in the dominant flow equation. This term accounts for active control of the system and provides a mechanism for modifying transport intensity and stability properties. The resulting evolution equation for the dominant transport mode is therefore constructed as a balance between linear growth or decay, nonlinear saturation, coupling with concentration dynamics, and external forcing. This yields

$$\frac{da_1}{dt} = \sigma a_1 - \alpha_1 a_1^3 - \alpha_2 a_1 a_2 + Q \quad (18)$$

where σ represents the net linear growth rate of the dominant transport structure, α_1 characterizes nonlinear self-limiting effects, and α_2 quantifies coupling strength between flow and CO_2 concentration. The CO_2 concentration mode evolves under the combined influence of advective transport, nonlinear saturation due to finite absorption capacity, and feedback from both flow and auxiliary mechanisms. Linear growth or accumulation of CO_2 is represented by a term proportional to a_2, while saturation effects arising from limited absorption capacity are modeled through a cubic damping term. The influence of flow-enhanced mixing is captured through a positive coupling term proportional to a_1, reflecting increased transport efficiency under stronger fluid motion. Additionally, interaction with the auxiliary mode introduces a damping contribution representing removal or redistribution effects. This leads to

$$\frac{da_2}{dt} = r a_2 - \beta_1 a_2^3 + \beta_2 a_1 - \beta_3 a_3 \quad (19)$$

where r denotes the net accumulation rate of CO_2, β_1 represents nonlinear saturation strength, β_2 quantifies flow-driven transport enhancement, and β_3 represents coupling with the stabilizing auxiliary mode. The third equation models a secondary transport or damping mechanism that captures delayed system response, absorber regeneration dynamics, or energy dissipation pathways not directly represented in the primary flow and concentration modes. This mode is assumed to relax toward equilibrium with a characteristic rate q, while being driven by CO_2 concentration and suppressed by nonlinear flow effects. The coupling from CO_2 concentration reflects delayed mass transfer into the auxiliary subsystem, while the quadratic dependence on flow represents nonlinear redistribution or damping induced by strong transport activity. This yields

$$\frac{da_3}{dt} = -q a_3 + \gamma_1 a_2 - \gamma_2 a_1^2 \quad (20)$$

© 2026 The Author(s) Licensed under CC BY 4.0 |

International Journal of Engineering, Science and Environment
Peer-Reviewed Open Access • CC BY 4.0 • Quarterly
ijese.in
Vol. 1 | Issue 2 | Jul–Sep 2026

where q is a relaxation parameter, γ_1 measures coupling from CO_2 concentration to the auxiliary mode, and γ_2 quantifies nonlinear suppression due to flow intensity. Collecting these contributions results in a closed three-dimensional nonlinear dynamical system that captures the essential interactions between fluid transport, CO_2 dynamics, and stabilizing mechanisms under external forcing:

$$\begin{aligned}\frac{da_1}{dt} &= \sigma a_1 - \alpha_1 a_1^3 - \alpha_2 a_1 a_2 + Q \\ \frac{da_2}{dt} &= r a_2 - \beta_1 a_2^3 + \beta_2 a_1 - \beta_3 a_3 \\ \frac{da_3}{dt} &= -q a_3 + \gamma_1 a_2 - \gamma_2 a_1^2\end{aligned} \tag{21}$$

This reduced-order formulation retains the key nonlinear mechanisms governing carbon dioxide removal systems, including saturation effects, cross-mode coupling, and externally controlled forcing. Importantly, the model's structure can generate rich dynamical behavior, including multiple steady states, Hopf bifurcations, and limit cycles, which are characteristic of strongly coupled environmental fluid systems with feedback and control. The formulation also provides a mathematically consistent framework for subsequent bifurcation analysis and optimal control design, where the forcing parameter Q serves as a natural actuator for modifying system stability and performance. Tables 1 and 2 list the variable and parameter details.

Table 1: State variables of the reduced-order CO_2 removal model

Symbol	Variable Name	Physical Meaning	Units
$a_1(t)$	Flow/Transport Mode	Dominant fluid motion or shear-driven transport intensity	Dimensionless modal amplitude
$a_2(t)$	CO_2 Concentration Mode	Effective CO_2 concentration / mixing state	Dimensionless modal amplitude
$a_3(t)$	Auxiliary Transport Mode	Dissipative/lagged absorption or regeneration dynamics	Dimensionless modal amplitude
$Q(t)$	External Forcing (Control Input)	Operational control (pumping, suction, injection rate)	Dimensionless control amplitude

The nondimensional coefficients in Table 2 may be interpreted in terms of the competing physical transport mechanisms represented by conventional dimensionless groups. Parameters controlling the growth, damping, and nonlinear saturation of the fluid-transport mode reflect the balance among inertial transport, viscous dissipation, and buoyancy-driven forcing and are therefore conceptually related to Reynolds- and Rayleigh-type effects. The coefficients governing the CO_2 concentration and mixing mode represent the competition between advective transport and molecular diffusion and can be associated with Péclet-type behavior. The relative importance of momentum diffusion and species diffusion is correspondingly related to Schmidt-number effects. Coupling coefficients between the reduced-order modes represent interactions among fluid motion, CO_2 transport, and the auxiliary dissipative or regeneration dynamics. These associations provide a physical interpretation of the reduced-order coefficients but should not be regarded as one-to-one numerical definitions of Reynolds, Rayleigh, Péclet, or Schmidt numbers. Because the present model is a proof-of-concept reduced-order formulation and is not calibrated to a particular geometry, fluid system, or CFD dataset, a quantitative mapping to specific dimensional operating conditions is not imposed.

Table 2: Model parameters of the reduced-order system

Symbol	Parameter Name	Value	Physical Meaning	Units
σ	Linear Growth Rate	1.5	Net instability or amplification of flow mode	Dimensionless
α_1	Flow Nonlinear Saturation	2.5	Self-limiting nonlinear damping of flow	Dimensionless
α_2	Flow–CO_2 Coupling Strength	1.5	Interaction between flow and concentration	Dimensionless
r	CO_2 Growth/Decay Rate	1.8	Net accumulation rate of CO_2 mode	Dimensionless
β_1	CO_2 Saturation Coefficient	1.0	Nonlinear limiting effect in CO_2 concentration	Dimensionless
β_2	Flow-to-CO_2 Transfer Coefficient	1.2	Enhancement of CO_2 transport by flow	Dimensionless
β_3	Auxiliary Damping Coupling	0.8	Removal effect via stabilizing mode	Dimensionless
q	Relaxation Rate	2.0	Decay rate of auxiliary mode	Dimensionless
γ_1	CO_2 → Auxiliary Coupling	0.17	Transfer from CO_2 to stabilizing mode	Dimensionless
γ_2	Flow-Induced Damping	0.5	Nonlinear suppression from strong flow	Dimensionless

The parameter values listed in Table 2 are representative nondimensional reduced-order model parameters and are not obtained from direct calibration against a specific experimental or CFD data set. They are selected to provide a dynamically meaningful test system exhibiting nonlinear saturation, intermodal coupling, multiple operating regimes, and oscillatory instability. Accordingly, the present model should be interpreted as a proof-of-concept reduced-order representation for investigating bifurcation-aware control methodology rather than as a quantitatively calibrated model of a particular CO_2 removal device. The bifurcation locations and optimal-control results reported below therefore apply to the present reduced-order model. Calibrating the reduced coefficients using CFD simulations or experimental measurements from a specific CO_2 capture system is an important direction for future work.

5. METHODOLOGY (BIFURCATION ANALYSIS AND OPTIMAL CONTROL)

5.1. Bifurcation Analysis

Continuation and bifurcation computations were carried out using the MATLAB-based software MATCONT. Bifurcation analysis provides important insights into the mechanisms underlying the existence of multiple steady states and self-

© 2026 The Author(s) Licensed under CC BY 4.0

sustained oscillations in nonlinear dynamical systems. In particular, branch points and limit points are associated with the emergence of multiple steady-state solutions, whereas oscillatory dynamics and periodic solutions originate from Hopf bifurcations. The package, originally developed and subsequently enhanced by several researchers, enables the systematic identification of limit points (LP), branch points (BP), and Hopf bifurcation points (H) in nonlinear dynamical models [31]. The package handles a system of ordinary differential equations

$$\frac{dx}{dt} = f(x,\alpha) \tag{22}$$

$x \in R^n$ where the bifurcation parameter is α .

At a limit point, the $n+1$ th component of the tangent vector $w_{n+1} = 0$. For a branch point,

the matrix $B = \begin{bmatrix} A \\ w^T \end{bmatrix}$ must be singular and have a determinant of 0.

At a Hopf bifurcation point,

$$\det(2 f_x(x,\alpha) @ I_n) = 0 \tag{23}$$

$@$ indicates the bialternate product while I_n is the n-square identity matrix. More details can be found in Kuznetsov and Govaerts [32,33].

5.2. Optimal Control

Pyomo.DAE [34] is used for the Optimal Control calculations. Pyomo with its Pyomo.DAE module provides an efficient framework for the formulation and solution of dynamic optimization problems involving systems of differential and algebraic equations. The package provides a symbolic modeling environment for representing differential-algebraic equation (DAE) systems in optimization applications. In Pyomo.DAE, the continuous-time dynamic model is transformed into a nonlinear programming (NLP) problem through discretization techniques such as orthogonal collocation, allowing the resulting optimization problem to be solved using standard NLP solvers. The NLP is solved using IPOPT [35]. The control problem is solved over a finite time horizon $0 \le t \le T$, where T denotes the final simulation time. The same time horizon is used for the control cases with and without the stability penalty to ensure a consistent comparison of the resulting objective values and control trajectories. The selected horizon is sufficiently long to capture the transient response of the reduced-order system and the effect of the control action.

The optimal-control objective was formulated to minimize the magnitudes of the dominant reduced-order state variables together with the effort associated with the external forcing. In continuous form, the objective without the stability penalty is expressed as

$$J_0 = \int_0^{t_f} \left[w_1 a_1(t)^2 + w_2 a_2(t)^2 + w_3 a_3(t)^2 + w_Q Q(t)^2 \right] dt. \tag{24}$$

For the calculations presented in this work, the state and control weighting parameters were selected as $w_1 = 1$, $w_2 = 1$, $w_3 = 0$, and $w_Q = 0.01$. Therefore, the continuous objective without the stability penalty becomes

$$J_0 = \int_0^{t_f} \left[a_1(t)^2 + a_2(t)^2 + 0.01 Q(t)^2 \right] dt. \tag{25}$$

The choice $w_3 = 0$ indicates that the auxiliary state $a_3(t)$ is not directly penalized in the objective function. Its evolution remains governed by the reduced-order dynamic equations and its coupling with the other state variables.

To incorporate stability information into the optimal-control formulation, an additional penalty based on the neural-network prediction of the maximum real part of the system eigenvalues was introduced. The stability-aware continuous objective is written as

$$J = \int_0^{t_f} \left[w_1 a_1(t)^2 + w_2 a_2(t)^2 + w_3 a_3(t)^2 + w_Q Q(t)^2 + W_s P(t)^2 \right] dt, \tag{26}$$

where $P(t) = \text{smooth}_{\text{m}}\text{ax}\left(\hat{\lambda}_{\max}(t)\right)$,

and $\hat{\lambda}_{\max}(t)$ is the stability indicator predicted by the neural-network surrogate. The stability penalty weight was selected as $W_s = 10$. This parameter corresponds to α_2 in the numerical implementation and controls the relative importance assigned to avoiding dynamically unstable regions. For the case without the stability penalty, $W_s = 0$.

Following temporal discretization, the objective implemented in Pyomo.DAE is represented as

$$J_d = \sum_{k=1}^{N} \left[w_1 a_{1,k}^2 + w_2 a_{2,k}^2 + w_3 a_{3,k}^2 + w_Q Q_k^2 + W_s P_k^2 \right],$$

where k denotes a discretized time point and N is the total number of discretized time points generated by the orthogonal-collocation procedure. Using the weights employed in the stability-aware calculations, the discretized objective becomes

$$J_d = \sum_{k=1}^{N} \left[w_1 a_{1,k}^2 + w_2 a_{2,k}^2 + w_3 a_{3,k}^2 + w_Q Q_k^2 + W_s P_k^2 \right], \tag{27}$$

with $P_k = \text{smooth}_{\text{m}}\text{ax}\left(\hat{\lambda}_{\max,k}\right)$.

For comparison, when the stability penalty is omitted, $W_s = 0$, and the discretized objective reduces to

$$J_{d,0} = \sum_{k=1}^{N} \left[a_{1,k}^2 + a_{2,k}^2 + 0.01 Q_k^2 \right]. \tag{28}$$

Here, w_1 and w_2 specify the relative penalties on the dominant fluid-transport and CO_2 concentration/mixing modes, respectively; w_3 determines the penalty on the auxiliary state; w_Q determines the penalty associated with the external control effort; and W_s controls the strength of the stability penalty.

5.3. Formation of Stability Dataset from MATCONT Results

A stability dataset was developed from numerical continuation calculations performed in MATCONT. The stability dataset consists of rows, each representing a continuation point from an equilibrium branch. Each row contains the state variables, the bifurcation parameter, and a stability measure. The

stability measure is a numerical value derived from the Jacobian matrix. The Jacobian matrix is computed numerically at each equilibrium point. The eigenvalues are then computed automatically using MATLAB. The maximum value of the real part of these eigenvalues is then computed as a scalar stability measure.

The stability measure is computed using "eig_real_max = max(real(eigvals));" in MATLAB. The stability measure is a quantitative metric in which negative values indicate locally asymptotically stable equilibria and positive values indicate instability. A zero crossing of the maximum real part indicates a change in local stability but does not, by itself, uniquely identify the type of bifurcation. A Hopf bifurcation occurs when a complex-conjugate pair of eigenvalues crosses the imaginary axis with nonzero imaginary parts, whereas a zero crossing associated with a real eigenvalue may correspond to a limit point or another steady-state bifurcation. The specific bifurcation type is therefore identified using the MATCONT continuation analysis. The stability dataset is then saved as a CSV file. The dataset can then be used in subsequent computational calculations to perform classification or regression to identify stability boundaries or approximate bifurcations.

5.4. Neural Network Surrogate for Stability Prediction

Direct embedding of eigenvalue calculations into IPOPT-based optimal control is impractical for several reasons: (i) computing eigenvalues at each time step is computationally expensive, (ii) the mapping from states to the maximum eigenvalue is non-smooth near eigenvalue crossings, and (iii) symbolic differentiation of eigenvalues is challenging.

To overcome these limitations, a feedforward neural network is trained to approximate the maximum eigenvalue as a smooth function of the system state and bifurcation parameter. A typical architecture employs the hyperbolic tangent (tanh) as a smooth activation function.

Prior to neural-network training, all input variables were standardized to improve numerical conditioning and training stability. Let x_{raw} denote the vector of state variables and bifurcation parameters obtained from the stability dataset. For each input variable j, the training mean μ_j and training standard deviation σ_j were computed over all training samples. The training mean for the input variable j is defined as the arithmetic average over all training samples as

$$\mu_j = \frac{1}{N}\sum_{k=1}^{N} x_j^{(k)}$$

and the training standard deviation for the input variable j is defined as:

$$\sigma_j = \frac{1}{N}\left(\sum_{k=1}^{N} x_j^{(k)} - \mu_j\right)^2$$

The standardized inputs were defined as

$$x_j = \frac{x_{raw,j} - \mu_j}{\max(\sigma_j, \varepsilon_{scale})} \tag{29}$$

where $\varepsilon_{\text{scale}}$ is a small positive regularization parameter introduced to prevent numerical singularities associated with extremely small variances. This transformation ensures that all inputs remain properly scaled while avoiding excessively large neural-network activation arguments during optimization. The normalization procedure improves neural-network conditioning and enhances the robustness of gradient-based optimization. The vectors μ and σ computed during training were stored and embedded identically within the Pyomo optimal-control formulation to ensure consistency between neural-network training and deployment.

If the input vector is denoted by x, which contains the scaled variables, the network architecture is defined as

$$\begin{aligned} z1 &= tanh(W1\,x + b1) \\ z2 &= tanh(W2\,z1 + b2) \\ \lambda_max_NN &= W3\,z2 + b3 \end{aligned} \tag{30}$$

where W_i and b_i denote the weight matrices and bias vectors, respectively. The hidden-layer variables z_1 and z_2 represent nonlinear transformations of the input variables and intermediate features. The final output $\hat{\lambda}_{\max}$ provides a smooth approximation of the spectral abscissa. Because tanh is infinitely differentiable, the network is fully smooth, guaranteeing the availability of first and second derivatives required by IPOPT. Without biases, the network output would be constrained to pass through the origin, limiting flexibility.

The hidden-layer outputs z_1 and z_2 represent nonlinear combinations of the inputs and previous-layer features, respectively. Each element of z_1 is a smoothed combination of the original inputs, while each element of z_2 encodes more abstract patterns extracted from z_1. The final output λ_max_NN provides a smooth approximation of the maximum real eigenvalue, enabling efficient and differentiable stability evaluation within the optimal control problem. The integration into optimal control is done using a soft penalty formulation where we use a smooth_max function that converts λ into a smooth, nonnegative penalty that only "activates" when the system is unstable:

$$s_{\max}(\lambda+\varepsilon_1) = smooth-\max(\lambda+\varepsilon_1) = \frac{(\lambda+\varepsilon_1)+\sqrt{(\lambda+\varepsilon_1)^2+\varepsilon_1}}{2} \tag{31}$$

λ is the neural network's predicted maximum eigenvalue at the current state and parameter, while ε is a small positive safety margin to ensure differentiability. The soft penalty formulation involves the new objective function, where the original objective function $\sum optv(t)$ is modified to $\sum (optv(t) + \alpha_{hopf}.s_{\max}(\lambda+\varepsilon_1))^2$ α_{Hopf} controls how aggressively instability is penalized, and prevents numerical issues at exactly $\lambda = 0$ and slightly shifts the stability boundary. When α_{Hopf} is 0, no stability penalty is implemented. The goal is to minimize the objective function value while ensuring differentiability for IPOPT and avoiding non-smoothness in the optimization. This approach avoids repeated eigenvalue computations and provides a smooth, differentiable surrogate suitable for gradient-based optimization. Furthermore, this enables the incorporation of stability constraints into optimal

International Journal of Engineering, Science and Environment
Peer-Reviewed Open Access • CC BY 4.0 • Quarterly
ijese.in
Vol. 1 | Issue 2 | Jul–Sep 2026

control without explicitly computing eigenvalues during optimization

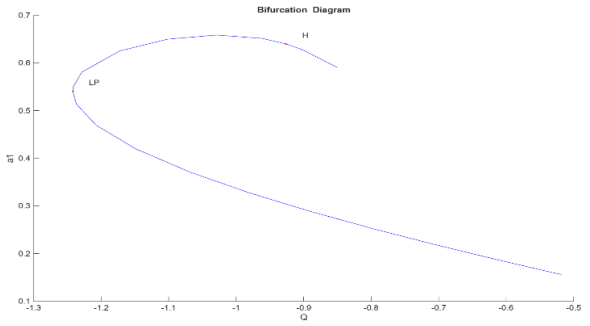


Fig. 1a. Bifurcation diagram

For reproducibility, the neural-network stability surrogate consists of four input variables, two hidden layers containing eight neurons each, and one output, giving an architecture of 4–8–8–1. The four inputs correspond to the three reduced-order state variables and the bifurcation parameter. Hyperbolic-tangent activation functions are used in both hidden layers, and the scalar output represents the predicted maximum real part of the system eigenvalues. The MATCONT continuation dataset contains 20 samples and was divided into 70% training data and 30% testing data, corresponding to 14 training samples and 6 testing samples.

The dynamic optimal-control problem was discretized using orthogonal collocation with 10 finite elements ($nfe = 10$) and 3 collocation points per finite element ($ncp = 3$). The initial conditions used for the control calculations were $a_1(0) = -1,\quad a_2(0) = -1,\quad a_3(0) = 1,\quad Q(0) = 0.$ We used the same discretization and initial conditions for the control calculations with and without the stability penalty to ensure a consistent comparison.

To quantitatively evaluate the accuracy of the neural-network stability surrogate, the MATCONT continuation dataset containing 20 samples was divided into 70% training data and 30% independent testing data. The neural network consisted of four input variables, two hidden layers with eight neurons in each layer using hyperbolic-tangent activation functions, and one output representing the predicted maximum real part of the system eigenvalues, $\lambda_{\max}$. On the independent test set, the surrogate produced a mean squared error of $MSE = 0.0976$, a mean absolute error of $MAE = 0.2890$, and a coefficient of determination of $R^2 = 0.9549$. Classification of equilibrium stability according to the sign of $\lambda_{\max}$ resulted in an accuracy of 83.33%.

The predictive performance near the stability boundary was also examined. Because none of the independent test samples satisfied the initially selected criterion $|\lambda_{\max}| \le 0.05$, the three test samples having the smallest values of $|\lambda_{\max}|$ were used to assess near-boundary prediction accuracy. For these samples, the mean absolute error was $MAE_{\text{boundary}} = 0.2072$ and the mean squared error was $MSE_{\text{boundary}} = 0.05284$. These results demonstrate good overall agreement between the neural-network predictions and the MATCONT-derived stability indicator, while also indicating that prediction in the immediate vicinity of $\lambda_{\max} = 0$ is more sensitive to the limited number of available continuation samples. Additional continuation data concentrated near the zero-crossing region could further improve the resolution of the stability boundary.

6. RESULTS

The bifurcation performed with MATCONT revealed the existence of a Hopf bifurcation point (a_1, a_2, a_3, Q) values of (0.640072 −0.647550 −0.157465 −0.926245) with a first Lyapunov coefficient of −1.349333e+00 and a limit point at (a_1, a_2, a_3, Q) values (0.540927 −1.018410 −0.159715 −1.242028). Figs. 1a and 1b show the bifurcation diagram and the limit cycle.

The analytical expression of the Jacobian matrix is

$$Ja = \begin{bmatrix} \sigma - 3\alpha_1 a_1^2 - \alpha_2 a_2 & -\alpha_2 a_1 & 0 \\ \beta_2 & r - 3\beta_1 a_2^2 & -\beta_3 \\ -2\gamma_2 a_1 & \gamma_1 & -q \end{bmatrix} \tag{32}$$

The numerical Jacobian at the Hopf bifurcation point is

$$Jn = \begin{bmatrix} -0.60136203648 & -0.960108 & 0 \\ 1.2 & 0.5400839925 & -0.8 \\ -0.640072 & 0.17 & -2 \end{bmatrix} \tag{33}$$

The eigenvalues of this matrix are −2.05936 and ±1.04016i. The presence of the complex conjugate eigenvalues on the imaginary axis indicates the presence of the Hopf bifurcation at this point.

The objective function is

$$\sum optv(t) = \sum (a_1(t))^2 + a_2(t))^2 + 0.01*(Q(t))^2$$

The optimal control problem was solved both without and with the stability-aware penalty.

This objective function penalizes the dominant fluid-transport mode a_1, the CO_2 concentration/mixing mode a_2, and the external control effort Q, thereby promoting reduced state deviations and lower control effort. To investigate the effect of stability-aware operation, the optimal control problem was solved both without and with the stability-aware penalty using Pyomo.DAE coupled with IPOPT.

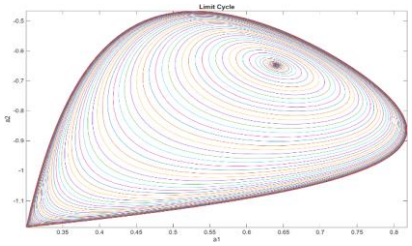


Fig. 1b. Limit cycle

When the stability penalty was omitted, the optimization produced an objective-function value of 148.606. When the neural-network-based stability penalty was included, the corresponding stability-aware objective-function value was 10.9422. Because the two formulations contain different

© 2026 The Author(s) Licensed under CC BY 4.0 | Published by Engineering, Science and Environmental Research Publications | e-ISSN 2839-5360 | ijese.in

International Journal of Engineering, Science and Environment
Peer-Reviewed Open Access • CC BY 4.0 • Quarterly
ijese.in
Vol. 1 | Issue 2 | Jul–Sep 2026

objective terms, these values are reported separately rather than interpreted as a direct percentage reduction in the same objective function.

The two optimal solutions nevertheless differ markedly, indicating the effect of the Hopf stability penalty on the optimal trajectory.

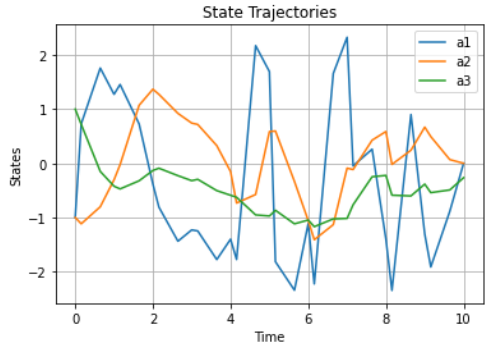


Fig. 2a. Optimal control state trajectory without stability penalty

This reduction should be interpreted as a model-specific demonstration of the potential benefit of the stability-aware control strategy rather than as a quantitatively validated performance improvement for a particular CO_2 removal device.

Figs. 2a and 2b show the optimal control state trajectory and control profile without the stability penalty, and Figs. 3a and 3b show the optimal control state trajectory and control profile with the stability penalty. A comparison of Figs. 2b and 3b shows a considerable reduction in the number of spikes when the Hopf stability penalty is included.

7. DISCUSSION

The reduced-order model developed for carbon dioxide removal exhibits a rich nonlinear structure that captures essential features of coupled fluid–reaction–transport dynamics. Despite its compact formulation, the system incorporates strong nonlinearities through cubic self-limiting terms, quadratic coupling between flow and concentration modes, and a control input that directly influences the dominant flow structure. This combination produces a highly nontrivial dynamical landscape characterized by equilibrium multiplicity, oscillatory instabilities, and sensitivity to parameter variations. Numerical continuation, eigenvalue analysis, and optimal control optimization provide a coherent picture of how the underlying bifurcation structure governs carbon dioxide removal performance.

The bifurcation analysis performed using numerical continuation reveals a well-defined equilibrium branch with embedded critical points. A key feature of this structure is the presence of a Hopf bifurcation at $(a_1, a_2, a_3, Q) = (0.640072, -0.647550, -0.157465, -0.926245)$, where the first Lyapunov coefficient is negative, indicating a supercritical Hopf bifurcation. This implies that the transition from steady-state behavior to oscillatory dynamics occurs smoothly, yielding a stable limit cycle rather than unstable divergence. From a physical perspective, this behavior corresponds to the onset of sustained oscillations in the CO_2 removal process, where interactions between advective transport (modeled by (a_1)) and concentration dynamics (a_2) become phase-locked, producing periodic variations in system performance.

The eigenvalue structure of the Jacobian at the Hopf bifurcation point provides further insight into the mechanism of instability. The eigenvalues are -2.05936 and $\pm 1.04016i$. Thus, a complex-conjugate pair lies on the imaginary axis at the Hopf point, consistent with the Hopf bifurcation identified by MATCONT. The third eigenvalue is negative, corresponding to a stable decaying mode. The periodic solution computed from the Hopf point further confirms the emergence of limit-cycle behavior.

At the Hopf bifurcation point, the complex-conjugate eigenvalue pair has zero real part and nonzero imaginary parts, placing the pair on the imaginary axis and satisfying the characteristic eigenvalue condition for a Hopf bifurcation.

The third eigenvalue, approximately (-2.059), is strongly negative, indicating a fast-decaying stable mode associated with the auxiliary variable (a_3). This separation of time scales implies that the essential dynamics of the system near the Hopf bifurcation are effectively two-dimensional, governed primarily by the interaction between (a_1) and (a_2), while (a_3) acts as a stabilizing dissipative mechanism.

In addition to the Hopf bifurcation, the equilibrium branch also exhibits a limit point, indicating the presence of a saddle-node bifurcation. This suggests that the system admits multiple steady-state solutions for certain ranges of the control parameter (Q), leading to potential multistability. From a carbon dioxide removal perspective, this is particularly significant, as it implies that the system may abruptly transition between qualitatively different operating regimes depending on initial conditions or external perturbations. Such behavior is characteristic of nonlinear transport systems where feedback between flow intensity and concentration fields leads to folded equilibrium manifolds. In practical terms, this means that the system may exhibit hysteresis, where recovery from a degraded state requires significantly different control actions than those required to maintain normal operation.

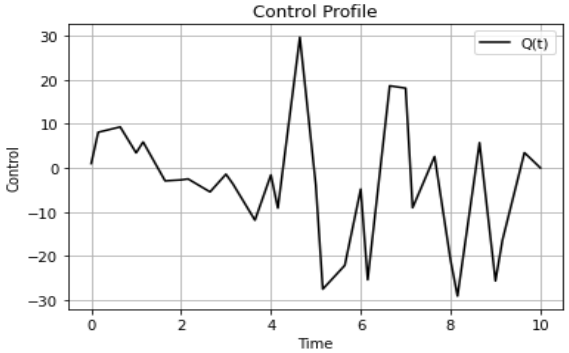


Fig. 2b. Optimal control profile without stability penalty

© 2026 The Author(s) Licensed under CC BY 4.0 |

International Journal of Engineering, Science and Environment
Peer-Reviewed Open Access • CC BY 4.0 • Quarterly
ijese.in
Vol. 1 | Issue 2 | Jul–Sep 2026

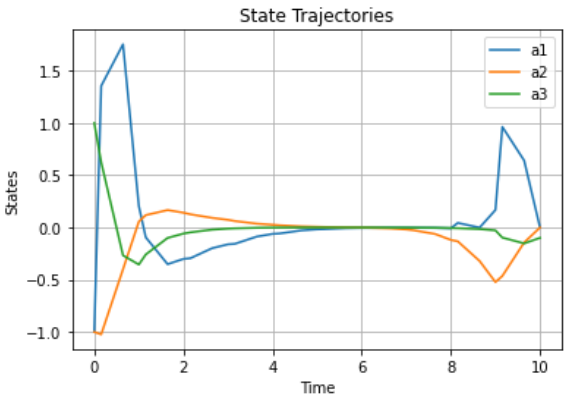


Fig. 3a. Optimal control state trajectory with stability penalty

The combined presence of Hopf and saddle-node bifurcations indicates that the carbon dioxide removal system operates near a critical regime where both oscillatory instability and multistability are possible. This type of structure is commonly observed in nonlinear fluid systems, particularly those involving coupled transport and reaction mechanisms. In the present model, the nonlinear coupling terms (a_1, a_2) and ($(a_1)^2$) are primarily responsible for generating these effects, as they introduce nonlinear feedback loops that can either amplify or suppress perturbations depending on the local state of the system.

To understand how these dynamical features influence system performance, an optimal control framework was introduced. The objective function penalizes the squared magnitude of the flow mode (a_1), the CO_2 concentration mode (a_2), and the control input (Q(t)). This structure corresponds to minimizing both the energetic content of the system and the external actuation effort required to maintain operation. Physically, this can be interpreted as seeking a low-energy operating regime in which carbon dioxide removal is achieved efficiently without excessive forcing or internal oscillations. The quadratic nature of the cost function ensures smoothness and convex-like behavior locally, although the underlying system dynamics remain highly nonlinear.

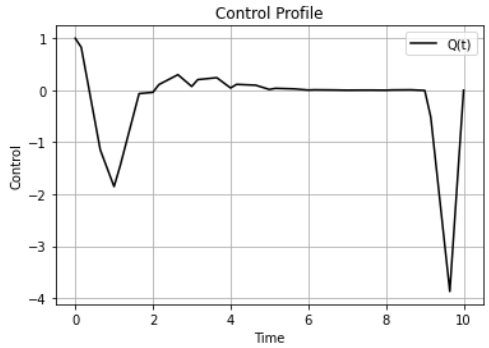


Fig. 3b. Optimal control profile with stability penalty

A key extension of the optimal control formulation is a stability-aware penalty based on a learned indicator of dynamical instability. This term penalizes trajectories that approach regions of state space associated with positive real parts of eigenvalues, effectively discouraging the system from entering neighborhoods of the Hopf bifurcation. From a dynamical systems perspective, this introduces bifurcation-aware control, where the optimizer considers not only instantaneous energy costs but also the trajectory's long-term stability properties. This modification substantially reshapes the optimal trajectory away from oscillatory regimes and toward more stable operating regions.

The numerical results demonstrate that inclusion of the stability penalty substantially changes the optimal-control solution. Without the stability penalty, the optimization produced an objective-function value of 148.606, whereas the stability-aware formulation produced an objective-function value of 10.9422. Because the stability-aware formulation contains an additional penalty term, these values correspond to different objective functions and are therefore not interpreted as a direct percentage reduction. The stability-aware solution nevertheless produced a noticeably smoother control profile. This suggests that avoiding proximity to the bifurcation boundary can promote smoother and more stable operation.

The reduction in control effort is further reflected in the smoothness of the optimal control profiles. Without the stability penalty, the control input shows high-frequency fluctuations, suggesting the system is actively counteracting unstable modes. These fluctuations are undesirable from an engineering standpoint, as they increase actuator wear and reduce efficiency. When the stability penalty is included, the control input becomes significantly smoother and lower in amplitude, indicating that the system naturally evolves within a more stable region of the state space that requires less corrective action. This demonstrates an important principle in nonlinear control: stabilizing the underlying dynamics can be more efficient than continuously compensating for instability through external forcing.

From a carbon dioxide removal perspective, these findings have important implications. The system shows that efficient CO_2 capture depends not only on control magnitude but also on the underlying dynamical regime in which the system operates. Operating near the Hopf bifurcation leads to oscillatory behavior that degrades performance and increases control effort, whereas operating in stable regions away from bifurcation boundaries leads to smoother dynamics and lower energy consumption. This suggests that optimal design of carbon capture systems should explicitly incorporate bifurcation structure, rather than relying solely on classical steady-state optimization.

Furthermore, the interplay between flow mode (a_1) and concentration mode (a_2) highlights the importance of feedback mechanisms in determining system performance. The Hopf bifurcation arises precisely from the interaction between these two modes, where energy transfer between flow and concentration fields leads to phase-shifted oscillations. The auxiliary variable (a_3) provides damping but does not fundamentally alter the instability mechanism. Instead, it modulates the amplitude and stability margin of the oscillations. This separation of roles suggests that targeted control strategies could focus specifically on modifying the

© 2026 The Author(s) Licensed under CC BY 4.0 |

coupling strength between (a_1) and (a_2) to suppress oscillatory behavior more effectively.

Overall, the results demonstrate that the reduced-order model captures essential features of carbon dioxide removal dynamics, including nonlinear feedback, multistability, oscillatory instability, and control-dependent stability transitions. The integration of bifurcation analysis with optimal control provides a powerful framework for understanding and improving system performance. In particular, the marked change in the optimal solution under stability-aware control highlights the importance of incorporating dynamical systems theory into the design of carbon capture processes. This approach not only improves efficiency but also enhances robustness by steering the system away from critical instability boundaries.

The present study provides a significant contribution to the understanding and control of carbon dioxide removal systems through the integration of nonlinear reduced-order modeling, bifurcation analysis, and optimal control. Unlike conventional approaches that treat CO_2 removal as a quasi-steady transport process, this work demonstrates that even simplified dynamical representations can exhibit rich nonlinear behavior, including Hopf bifurcations, limit cycles, and multistability. These features are crucial because they directly influence the operational stability and efficiency of carbon capture processes.

One of the most important impacts of this work is the identification of a clear instability boundary governed by a Hopf bifurcation, which separates steady operating regimes from oscillatory CO_2 dynamics. In practical carbon dioxide removal systems, such oscillations can correspond to periodic fluctuations in capture efficiency, mixing intensity, or reactor performance. By explicitly characterizing the location of this bifurcation in state–parameter space, the study provides a predictive framework for avoiding undesirable oscillatory regimes during system design and operation. This is particularly relevant for engineered systems such as adsorption columns, membrane-based separators, or fluidized capture reactors, where nonlinear feedback mechanisms are often present but not explicitly modeled at the reduced-order level.

A second major impact lies in the demonstration that optimal control strategies are strongly dependent on underlying bifurcation structure. The results show that when control is designed without accounting for instability mechanisms, the system exhibits highly oscillatory and energetically inefficient behavior. In contrast, incorporating a bifurcation-aware penalty substantially changes the optimal solution and produces smoother, lower-amplitude control trajectories. This highlights a key principle: effective carbon dioxide removal is not solely achieved by minimizing instantaneous concentration levels, but by shaping the dynamical regime in which the system operates.

The study also demonstrates the value of reduced-order modeling as a design tool for carbon capture systems. Despite its simplicity, the model captures essential nonlinear interactions between flow, concentration, and auxiliary transport modes, enabling the emergence of realistic dynamical phenomena. This suggests that reduced-order models can serve as efficient surrogates for more expensive PDE-based simulations when exploring control strategies, stability boundaries, and operational optimization. Furthermore, the integration of data-driven components, such as the neural-network-based stability indicator, introduces a pathway toward hybrid physics–machine learning control frameworks. This enables the system to learn regions of instability directly from continuation data and incorporate this knowledge into the optimization process. Such an approach is particularly promising for complex CO_2 removal systems where analytical stability conditions are difficult to derive.

Overall, this work advances carbon dioxide removal research by linking nonlinear dynamics, bifurcation theory, and optimal control into a unified framework. It provides both theoretical insight and practical methodology for designing more stable, efficient, and robust carbon capture processes operating near critical dynamical regimes.

8. CONCLUSION

This study developed and analyzed a reduced-order nonlinear dynamical model for carbon dioxide removal, incorporating coupled flow, concentration, and auxiliary transport modes with external forcing. The model captures essential nonlinear interactions through cubic saturation terms and quadratic coupling, enabling the emergence of rich dynamical behavior including multistability, oscillatory instability, and control-sensitive transitions. Numerical continuation using MATCONT revealed a clear bifurcation structure, consisting of a supercritical Hopf bifurcation and a saddle-node (limit point) bifurcation along the equilibrium branch.

The Hopf bifurcation occurs at
$(a_1, a_2, a_3, Q) = (0.640072, -0.647550, -0.157465, -0.926245)$
, where the system transitions from steady-state operation to stable periodic oscillations. Eigenvalue analysis confirms the Hopf bifurcation, with a complex-conjugate eigenvalue pair lying on the imaginary axis at the bifurcation point and a negative third eigenvalue corresponding to a stable decaying mode. The auxiliary variable acts as a stabilizing contribution but does not eliminate the fundamental oscillatory instability arising from nonlinear coupling between primary modes.

An optimal control framework was formulated to minimize the combined energy of system states and control effort, with an additional stability-aware penalty that discourages trajectories near the Hopf instability region. The results show that bifurcation-aware control substantially changes the optimal solution. Specifically, the objective-function value was 148.606 without the stability penalty and 10.9422 with the Hopf stability penalty; because the two formulations contain different objective terms, these values are reported separately rather than as a percentage reduction. The stability-aware solution is accompanied by significantly smoother control profiles and reduced high-frequency actuation.

The present study has several limitations that should be considered when interpreting the results. The reduced-order model is a proof-of-concept formulation based on representative nondimensional parameter values and has not

© 2026 The Author(s) Licensed under CC BY 4.0 | Published by Engineering, Science and Environmental Research Publications | e-ISSN 2839-5360 | ijese.in

been calibrated against a specific experimental or CFD dataset. In addition, the neural-network stability surrogate was developed using a relatively small MATCONT dataset consisting of 20 samples, with 14 samples used for training and 6 for testing. The resulting stability-classification accuracy of 83.33% should therefore be interpreted cautiously because it is based on a small test set. Future work will focus on generating larger continuation datasets, improving and validating the neural-network stability surrogate, and calibrating the reduced-order model using experimental measurements or high-fidelity CFD simulations for specific CO_2 removal systems.

DECLARATIONS

Acknowledgement

The author thanks Dr. Carlos Ramirez for his encouragement for writing single-author papers.

Author Contribution

L. N. Sridhar is the sole author of this work and confirms sole responsibility for the model formulation, numerical simulations, data analysis, and manuscript preparation.

Data Availability Statement

The numerical results presented in this study were generated using the reduced-order model and computational procedures described in the manuscript. The MATCONT continuation dataset and the neural-network implementation used for the stability analysis are available from the corresponding author upon reasonable request.

Conflict of Interest

The author, Dr. Lakshmi N. Sridhar, declares no conflict of interest.

Funding

No funding was received for this research.

REFERENCES

[1] P. H. M. Feron and C. A. Hendriks, "CO_2 capture process principles and costs," *Oil & Gas Science and Technology – Rev. IFP*, vol. 60, no. 3, pp. 451–459, 2005, doi: 10.2516/ogst:2005027.

[2] G. T. Rochelle, "Amine scrubbing for CO_2 capture," *Science*, vol. 325, no. 5948, pp. 1652–1654, 2009, doi: 10.1126/science.1176731.

[3] C. Tsouris and L. L. Tavlarides, "Breakage and coalescence models for drops in turbulent dispersions," AIChE Journal, vol. 40, no. 3, pp. 395–406, 1994, doi: 10.1002/aic.690400303.

[4] M. Wang, A. Lawal, P. Stephenson, J. Sidders, and C. Ramshaw, "Post-combustion CO_2 capture with chemical absorption: A state-of-the-art review," *Chemical Engineering Research and Design*, vol. 89, no. 9, pp. 1609–1624, 2011, doi: 10.1016/j.cherd.2010.11.005.

[5] G. F. Versteeg and W. P. M. van Swaaij, "Solubility and diffusivity of acid gases (CO_2, N_2O) in aqueous alkanolamine solutions," Journal of Chemical & Engineering Data, vol. 33, no. 1, pp. 29–34, 1988, doi: 10.1021/je00051a011.

[6] S. Bachu, "Sequestration of CO_2 in geological media: Criteria and approach for site selection in response to climate change," *Energy Conversion and Management*, vol. 41, no. 9, pp. 953–970, 2000, doi: 10.1016/S0196-8904(99)00149-1.

[7] M. Bui, C. S. Adjiman, A. Bardow, E. J. Anthony, A. Boston, S. Brown, et al., "Carbon capture and storage (CCS): The way forward," *Energy & Environmental Science*, vol. 11, no. 5, pp. 1062–1176, 2018, doi: 10.1039/C7EE02342A.

[8] H. E. Huppert and J. A. Neufeld, "The fluid mechanics of carbon dioxide sequestration," Annual Review of Fluid Mechanics, vol. 46, pp. 255–272, 2014, doi: 10.1146/annurev-fluid-011212-140627.

[9] J. Ennis-King and L. Paterson, "Coupling of geochemical reactions and convective mixing in the long-term geological storage of carbon dioxide," *International Journal of Greenhouse Gas Control*, vol. 1, no. 1, pp. 86–93, 2007.

[10] S. M. Benson and D. R. Cole, "CO_2 sequestration in deep sedimentary formations," *Elements*, vol. 4, pp. 325–331, 2008.

[11] B. Metz, O. Davidson, H. de Coninck, M. Loos, and L. Meyer, Eds., *IPCC Special Report on Carbon Dioxide Capture and Storage*. Cambridge, UK: Cambridge University Press, 2005.

[12] J. A. Neufeld, M. A. Hesse, A. Riaz, M. A. Hallworth, H. A. Tchelepi, and H. E. Huppert, "Convective dissolution of carbon dioxide in saline aquifers," *Geophysical Research Letters*, vol. 37, Art. no. L22404, 2010, doi: 10.1029/2010GL044728.

[13] C. W. MacMinn, M. L. Szulczewski, and R. Juanes, "CO_2 migration in saline aquifers. Part 1. Capillary trapping under slope and groundwater flow," *Journal of Fluid Mechanics*, vol. 662, pp. 329–351, 2010.

[14] R. Juanes, E. J. Spiteri, F. M. Orr Jr., and M. J. Blunt, "Impact of relative permeability hysteresis on geological CO_2 storage," *Water Resources Research*, vol. 42, Art. no. W12418, 2006, doi: 10.1029/2005WR004806.

[15] M. L. Szulczewski, C. W. MacMinn, H. J. Herzog, and R. Juanes, "Lifetime of carbon capture and storage as a climate-change mitigation technology," *Proceedings of the National Academy of Sciences of the United States of America*, vol. 109, no. 14, pp. 5185–5189, 2012, doi: 10.1073/pnas.1115347109.

[16] K. S. Lackner, "The thermodynamics of direct air capture of carbon dioxide," *Energy*, vol. 50, pp. 38–46, 2013.

[17] D. W. Keith, G. Holmes, D. St. Angelo, and K. Heidel, "A process for capturing CO_2 from the atmosphere," *Joule*, vol. 2, no. 8, pp. 1573–1594, 2018, doi: 10.1016/j.joule.2018.05.006.

[18] M. J. Bickle, "Geological carbon storage," *Nature Geoscience*, vol. 2, pp. 815–818, 2009, doi: 10.1038/ngeo687.

[19] H. J. Herzog, "Scaling up carbon dioxide capture and storage: From megatons to gigatons," *Energy Economics*, vol. 33, no. 4, pp. 597–604, 2011, doi: 10.1016/j.eneco.2010.11.004.

[20] C. Doughty and K. Pruess, "Modeling supercritical carbon dioxide injection in heterogeneous porous media," *Vadose Zone Journal*, vol. 3, no. 3, pp. 837–847, 2004.

[21] E. S. Sanz-Pérez, C. R. Murdock, S. A. Didas, and C. W. Jones, "Direct capture of CO_2 from ambient air," *Chemical Reviews*, vol. 116, pp. 11840–11876, 2016.

[22] J. M. Matter, M. Stute, S. O. Snæbjörnsdóttir *et al.*, "Rapid mineralization of carbon dioxide in basaltic formations," *Science*, vol. 352, pp. 1312–1314, 2016.

[23] D. A. Nield and A. Bejan, *Convection in Porous Media*, 5th ed. Springer, 2017.

[24] A. S. Denning, I. Y. Fung, and D. Randall, "Latitudinal gradient of atmospheric CO_2 due to seasonal exchange with land biota," *Nature*, vol. 376, pp. 240–243, 1995, doi: 10.1038/376240a0.

[25] J. Wilcox, *Carbon Capture*. New York, NY, USA: Springer, 2012.

[26] M. Fajardy and N. Mac Dowell, "The energy return on investment of BECCS: Is BECCS a threat to energy security?," *Energy & Environmental Science*, vol. 11, no. 6, pp. 1581–1594, 2018, doi: 10.1039/C7EE03610H.

[27] C. Breyer, M. Fasihi, C. Bajamundi, and F. Creutzig, "Direct air capture of CO_2: A key technology for ambitious climate change mitigation," *Joule*, vol. 3, no. 9, pp. 2053–2057, 2019.

© 2026 The Author(s) Licensed under CC BY 4.0 |

[28] J. C. Abanades, B. Arias, A. Lyngfelt, T. Mattisson, D. E. Wiley, H. Li, et al., "Emerging CO_2 capture systems," *International Journal of Greenhouse Gas Control*, vol. 40, pp. 126–166, 2015.

[29] S. M. Smith, O. Geden, G. F. Nemet, M. W. Gidden, W. F. Lamb, C. Powis, et al., *The State of Carbon Dioxide Removal*, 1st ed., 2023, doi: 10.17605/OSF.IO/W3B4Z.

[30] A. Parkash, A. Kadier, and P.-C. Ma, "Copper-deposited basalt fiber fabric for electrochemical CO_2 reduction to ethanol with 98% selectivity," *Energy*, vol. 327, Art. no. 136453, 2025.

[31] A. Dhooge, W. Govaerts, and Y. A. Kuznetsov, "MATCONT: A MATLAB package for numerical bifurcation analysis of ODEs," *ACM Transactions on Mathematical Software*, vol. 29, no. 2, pp. 141–164, 2003.

[32] Y. A. Kuznetsov, *Elements of Applied Bifurcation Theory*. New York, NY, USA: Springer, 1998.

[33] W. J. F. Govaerts, *Numerical Methods for Bifurcations of Dynamical Equilibria*. SIAM, 2000.

[34] W. E. Hart, C. D. Laird, J.-P. Watson, D. L. Woodruff, G. A. Hackebeil, B. L. Nicholson, and J. D. Siirola, *Pyomo – Optimization Modeling in Python*, 2nd ed., vol. 67. Springer, 2017.

[35] A. Wächter and L. T. Biegler, "On the implementation of an interior-point filter line-search algorithm for large-scale nonlinear programming," *Mathematical Programming*, vol. 106, pp. 25–57, 2006, doi: 10.1007/s10107-004-0559-y.

© 2026 The Author(s) Licensed under CC BY 4.0 | Published by Engineering, Science and Environmental Research Publications | e-ISSN 2839-5360 | ijese.in